Available online at www.sciencedirect.com

ScienceDirect

Procedia Structural Integrity 2 (2016) 3617–3624

Structural Integrity Procedia

www.elsevier.com/locate/procedia

21st European Conference on Fracture, ECF21, 20-24 June 2016, Catania, Italy

High strain rate behavior of aluminum die cast components

G.Ubertalli[a], F. D'Aiuto[b], S. Plano[b], D. De Caro[a]*

[a]*Politecnico di Torino, Corso Duca degli Abruzzi 24, Torino 10137, Italy*
[b]*Centro Ricerche FIAT, Torino 10135, Italy*

Abstract

Research results of static and dynamic mechanical tests ($\dot{\epsilon} = 1 * 10^{-3}\, s^{-1}$ and $\dot{\epsilon} \sim 5 * 10^{2}\, s^{-1}$) conducted on samples obtained from three different die cast products (component A, B and C) of AlSi10MnMg alloy are reported. All the components have thin-walled geometry except some thicker positions of component C. The dynamic (high strain rate) mechanical characterization shows an increase of tensile properties, in respect to static tensile ones (tensile strength increases approximately 15%, and the yield strength 30%, for all the die cast components) together with an evident plastic deformation, with consequent necked region in the fractured section, substantially negligible in case of static tensile tests.
Moreover, fractographic observations are conducted on specimens undergone static and high strain rate test conditions, to observe the fracture morphology, together with metallographic analysis on the only polished or etched transverse specimens to reveal the porosity, and the microstructure of dendrite and inter-dendrite morphologies.

Peer-review under responsibility of the Scientific Committee of ECF21.

Keywords: High strain rate test; die cast aluminum alloy; fracture morphology; porosity.

1. Introduction

In an effort to improve the fuel efficiency of automobiles, car designers are investigating new materials to reduce the overall vehicle weight, by the substitution of steel and iron casting components by plastics, carbon fibres, or aluminium and magnesium alloys; currently more than 60% of vehicle weight is due to use of steel or cast iron in the body structure. Aluminium alloys are good candidates to achieve that weight reduction due in part to their low density and high specific strength, Shultz et al. (2008).

* Corresponding author. Tel.: +39-011-090-4634; fax: +39-011-090-4624.
E-mail address: daniele.decaro@polito.it

Peer review under responsibility of the Scientific Committee of ECF21.
10.1016/j.prostr.2016.06.451

Nowadays aluminium components produced by pressure die casting technology are used for many automotive applications such as shock tower, engine bracket, front-end carrier, instrument panel, Franke et al. (2007), Kaufman et al. (2004).

This technology is particularly suitable for high production rates, it is economically feasible for large production series (more than about 5,000-10,000 parts/year) of complex thin-walled components requiring strict dimensional tolerance and good surface finishing. For these reasons, approximately half of the world production of light metal castings is obtained by this technology, Vicario et al. (2016). One of the disadvantages is the almost inevitable presence of casting defects such as shrinkage cavities, often coupled with other defect types: cold fills, alumina skins, dross, entrapped air bubbles, Avalle et al. (2002), Càceres et al. (1996). On the other hand the high production frequency guaranteed by this technology induces a fine microstructure, however not homogeneous through the wall thickness, and a surface skin effect, which result as a benefit in final mechanical behaviour, Niklas et al. (2015), Ubertalli et al. (2015). The Al–Si–Mg systems (A300 series from the Aluminium Association Numbering System) are the most important alloys for casting products in automotive field from a commercial standpoint, sometime also for components that could be subjected to impulsive load during their life; several vehicle components are designed to work as energy absorbers in the event of crash, such that the deceleration seen by the driver is not so harsh to cause severe bodily injury. In order to know the dynamic properties of the materials, these must be tested in conditions that reproduce the actual working issues, Mirone (2013). Therefore dynamic material testing method-assuring results of high precision must be adopted, in order to understand the strain rate sensitivity of materials.

It is scientifically recognized that the most satisfactory testing method for accurate measurement of dynamic mechanical properties for materials is the Hopkinson bar technique, which allows the generation of a loading pulse well controlled in rise time, amplitude and duration, and producing a propagation of a uniaxial elastic plane stress wave, Kolsky (1949). Different versions of the Hopkinson bar technique were developed to investigate dynamic tensile properties of materials, Albertini et al. (1974).

In the literature, there is a lack of knowledge about the mechanical behaviour of aluminium alloys at high strain rates. Few studies were conducted by Vilamosa et al. (2015) about the thermo-mechanical behaviour in tension of three as-cast and homogenized Al-Mg-Si alloys (6060 and 6082 aluminium alloys) in a wide range of strain rates ($0.01 \div 750\ s^{-1}$) and temperatures ($20 \div 350$ °C). The authors evidence a slightly positive strain rates effect on flow stress at room temperature, and a more significant effect at temperatures higher than 250 °C. In addition, other authors investigated the mechanical properties of various aluminium wrought alloys at different strain rate conditions, Ma et al. (2014), Smerd et al. (2005), Tan et al. (2015). However, no works are found in literature about the dynamic characterization of die cast aluminium alloys.

The research investigates the static and dynamic behaviour of three different die cast products in AlSi10MnMg alloy together with metallographic and fractographic observations in order to correlate the obtained mechanical properties.

2. Experimental part

Three different components (in particular 2 pieces of product A, 2 of B and 3 of C) of car body, produced with die cast technology in AlSi10MnMg alloy, have been investigated. The components (one of these is shown in Fig. 1) were in T6 condition.

The three types of components, analyzed with optical emission spectroscopy (OES), show the chemical composition in wt. %, reported in Table 1. The chemical composition of the products are quite similar, and in accordance with UNI EN 1706 (EN AC 43500).

Table 1. Chemical composition.

Component	%Cu	%Si	%Fe	%Mn	%Mg	%Zn	%Ti	%Ni	%Pb	%Sn	%Cr	%Sr	%Al
A	0.01	10.8	0.15	0.60	0.30	0.01	0.05	<0.01	<0.01	<0.01	<0.01	0.010	Rest
B	0.01	10.8	0.12	0.65	0.29	0.03	0.06	<0.01	<0.01	<0.01	<0.01	0.010	Rest
C	0.03	10.9	0.19	0.51	0.33	0.03	0.05	0.01	<0.01	<0.01	<0.01	0.013	Rest

Fig. 1. Shock tower investigated in this work.

The weight of the components ranges from around 4.2 kg for the component A, to 4.8 kg for the component C; the difference in weight for the investigated products is mainly due to the slightly different geometry and, in some parts of the different components, different wall thickness.

The wall thicknesses of the components were measured, with ultrasonic system, in different positions; the minimum and maximum obtained values, for every component, are reported in Table 2.

Table 2. Minimum and maximum thickness measured.

Component	Min Thickness [mm]	Max Thickness [mm]
$A_{1,2}$	2.3	4.9
$B_{1,2}$	2.9	4
$C_{1,2,3}$	2.9	12

Wall thickness of all the components are substantially included in the range 2.9 ÷ 4 mm. The component A shows a slightly increase in this range as concerning minimum and maximum values, while the component C, in one part of it, has a considerably higher thickness.

Static and dynamic tensile tests were performed on the samples got from the component in number ranging from 8 to 12 depending on the component. The tensile static tests ($d\varepsilon/dt \sim 10^{-3}\ s^{-1}$) were performed by an electromechanical universal testing machine, 200 kN maximum load capacity. A mechanical extensometer was used in order to measure the strain on the specimen gauge length. The samples are flat, 42 mm gauge length, 8 mm width. As concerning the thickness, the samples are milled to produce test specimens 3 mm thick. In case of samples cut off in part with thinner thickness, the sample, of course, maintains this thickness and shows raw surfaces. In case of component C characterized, in some part, with larger thickness, core positions were also taken in account.

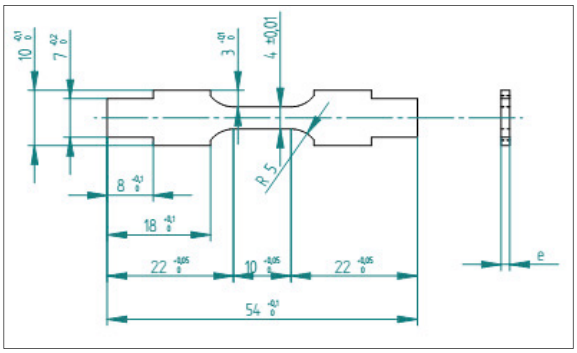

Fig. 2. Dynamic test specimen geometry.

The high strain rate tests, at 500 s^{-1}, were carried out on the modified Hopkinson bar device, the tension version developed by Albertini and Montagnani in seventies and nowadays widely used, Albertini et al. (1974). The tested specimens, taken off in positions next to those of the static test ones, are flat, 10 mm gauge length, 4 mm width and 2 mm thick; the geometry is shown in Fig. 2.

Brinell hardness tests HBW 2.5/62.5 were conducted, in accordance with the UNI EN ISO 6506-1 on the head of the tensile samples, before tests.

Samples for metallographic examination, 25 mm in length, were cut close to the zone analyzed for mechanical tests. The metallographic, only polished, samples underwent optical analysis (100 X magnification) to detect the porosity amount and distribution throughout five equidistant sections through the thickness. The acquired images were processed by image analysis software ImageJ, for the evaluation of areas, dimensions and shape of porosity. Only voids with area greater than 7.07 μm^2 (equivalent to a circular porosity of 3μm as diameter) were taken into consideration.

Furthermore, etched samples were observed to detect the microstructure and to evidence the phases and micro-constituents distribution and morphology, and the influence of different wall thicknesses.

The fracture morphologies of the samples undergone static and dynamic tests were observed with electron microscope.

3. Results and discussion

The microscopic observation of the transverse section of the un-etched samples evidences a certain amount of pores in all the samples observed. However, the calculation effected by image analysis software ImageJ yields results of area percentage that range from 0.005 % to 0.20 % in most parts of samples. Only in some samples of the C component the area percentage of pores reaches values of 0.70 %. Very different is the case of transverse section of thick – 12 mm – component C samples, in which the porosity % reaches the value of 1.5 % at average depths and 6 % average at core.

Pore area distribution follows a normal logarithmic curve. Pores appear generally elongated with a maximum to minimum dimension ratio that ranges between 1.3 e 2.4 and with a quite indented boundary.

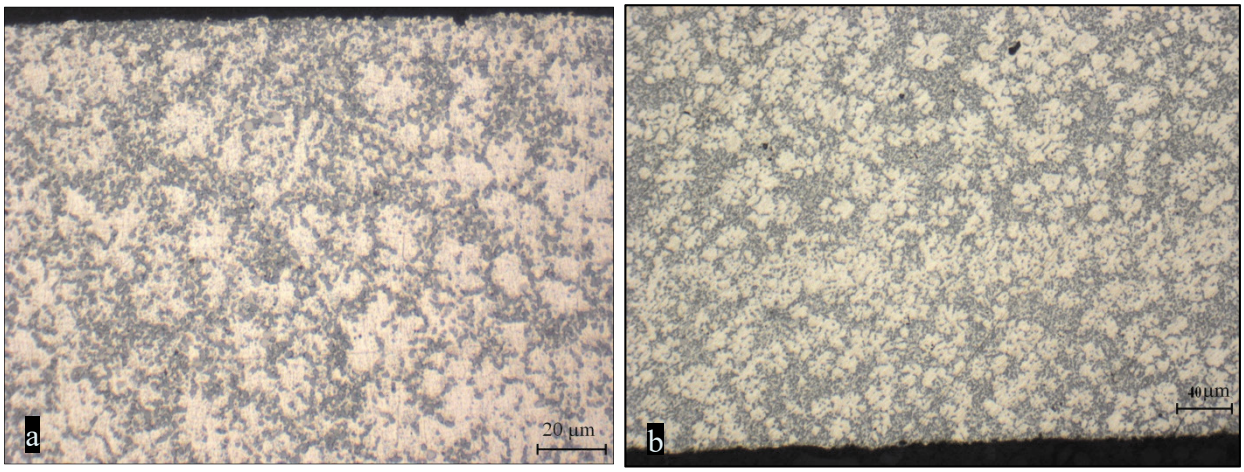

Fig. 3. Metallographic microstructure (a) of component B – 625X – Keller etching (b) Component C – 250X - Keller etching.

The metallographic transverse samples observed after Keller etching show a very fine dendritic morphology at the surface that progressively grows toward the center of the specimen thickness (Fig 3a). The Si particles are always fine and rounded. Some polygonal particles of phase (Al-Fe-Mn-Si), with a quite random distribution, are detected. However, in the component A some large dendrites are detected, together with fine ones, starting at 150 μm from the surface. The component C shows the higher amount of areas where a high percentage of interdendritic

microstructure (mixture of aluminium rich phase and silicon round particles) is present, almost until 1 mm from the surface (Fig. 3b). The component B shows the higher homogeneity in the microstructure and phase distribution (Fig. 3a).

The samples undergone static tensile test did not show any evident necking deformation at rupture. The plotted engineering curves confirm this behavior; in fact, for almost all the tested specimens, after that the tensile strength is reached, a fast load decreasing, followed by fracture, appears. The range of results obtained from static tensile tests are reported in table 3 as yield strength (*YS*), tensile strength (*TS*), and elongation to fracture (e_f %), for the three different components; the values of the component C are divided between small and high thickness.

Table 3. Results of static tensile tests.

Components		*TS* [MPa]	*YS* [MPa]	e_f %
$A_{1,2}$		175 ÷ 190	110 ÷ 125	7 ÷ 15
$B_{1,2}$		180 ÷ 195		11 ÷ 18
$C_{1,2,3}$	Thin wall (≈ 3 mm)	175 ÷ 195		7.5 ÷ 13.5
	Thick wall (12 mm)	155 ÷ 170		2.5 ÷ 4

The results show that the tensile and yield strength of the different components and sampling positions of each component are very similar (*TS* around 185 MPa and *YS* 115 MPa), also taking in to account some different surface distance, such as the values of the ranges obtained (around 15 MPa). Only in the case of component C with thick wall the strength values is lower and around 160 MPa.

Instead, the comparison among the three analyzed components shows bigger differences in the results of elongation at rupture. In fact the specimens taken from the component B show the highest values of engineering strain; component A and C (in this case, thin wall) show similar results, slightly lower than those of component B. On the contrary, the tensile samples got from thick wall position of component C exhibit the minimum engineering strain values, even one third of all the others thin wall components.

It is possible to explain this trend with a coarser microstructure and a higher porosity, typical of regions with high wall thickness.

However, it is necessary to underline that a very large data scattering was detected about the elongation results for all the components. This scattering is related not only to the different picking positions, but it also refers to analogous positions of identical pieces of the same component.

Raw data collected in the Hopkinson tensile experimental tests show evident damped oscillations of stress values in the true stress-strain curves as confirmed by many other researchers, Vilamosa et al. (2015), Singh et al. (2013). Raw data were therefore fitted according the Ludwik equation (1), in order to plot a continuous and smoothed curve in the true stress – plastic strain diagram, Ludwik (1909).

$$\sigma_{True} = C_0 + C_1 {\varepsilon_p}^m \tag{1}$$

Where:
σ_{True} = true stress
ε_p = true plastic strain
C_0, C_1, m = Ludwik equation parameters

The tensile strength and the yield strength (this latter detected at $\varepsilon_p = 0.002$ in the fitted curve), for components A, B and C, of dynamic tensile tests are reported in table 4 together with e_u % - uniform elongation percentage calculated as the elongation of tensile sample between *YS* and *TS* values and the (e_f - e_u) %, defined as fraction percentage of the strain of tensile sample beyond the *TS*, when necking appears.

The tensile and yield strength of the different components and sampling positions of each component are very similar (*TS* around 205 MPa, *YS* around 155 MPa respectively) for the different samples. The comparison between static and dynamic tensile results evidences better mechanical properties at high strain rate; however, the increase is not proportional with strain, as hereafter analyzed.

Table 4. Results of dynamic tensile tests.

Components		*TS* [MPa]	*YS* [MPa]	e_u %	(e_f - e_u) %
$A_{1,2}$		200 ÷ 210	148 ÷ 160	10 ÷ 12	35 ÷ 55
$B_{1,2}$		205 ÷ 215	150 ÷ 170	10 ÷ 15	25 ÷ 45
$C_{1,2,3}$	Small thickness (3 mm)	190 ÷ 205	150 ÷ 160	9 ÷ 11	35 ÷ 50
	High thickness (12 mm)			5 ÷ 7	20 ÷ 30

All samples tested in dynamic conditions show larger total elongation in comparison to static tensile ones. Even if the values e_f % of static and dynamic tests cannot be directly compared, because of the different geometry and dimensions of the calibrated section, the authors consider reasonable to divide the contribution of strain amount till TS and beyond it. The former part of total elongation shows that the values of e_u % (till *TS*) after dynamic tests are very similar to those obtained in the static test samples, excluding the results of C thick wall component. The fractions of strain beyond *TS* as percentage of total strain is the second contribution, reported in the last right column of Table 4. In the case of static tensile tests, this fraction was almost negligible (as in the plotted stress strain curves and in the macroscopic observation) and not reported in table 3 while, in the dynamic test, the specimens exhibit larger elongation evidenced by the pronounced necking zone visible on the broken specimens. The amount of calculated fraction of deformation beyond necking ((e_f - e_u) %) can reach 50 %. Other authors evidenced this behavior, observed on different sheet aluminium alloys, Ma et al. (2014), Smerd et al. (2005), Tan et al. (2015).

In order to examine in depth the increase of strength mechanical properties vs strain rate, the true dynamic stress - true static stress ratio (known as Dynamic Increase Factor – DIF as defined by D'Aiuto et al. (2015)) versus true plastic strain was calculated, for the couples of samples taken off from adjacent position. The results show that DIF, of the analyzed die cast aluminum alloy, ranges from 1.25 to 1.5 in case of true plastic strain of 0.004 (near the yield stress) and decreases to 1.1 – 1.15 as the true plastic strain is 0.04. Fig. 4 shows the minimum and maximum calculated DIF values in case of component A. All other samples of component A, show the same trend of DIF values vs true plastic strain and the calculated values stay in the range reported in Fig. 4. The specimens of component B and C evidence the same type of behaviour even if the DIF values can be slightly different.

The observed decrease of DIF ratio, by increasing true plastic strain, shows a progressive slope reduction to reach a minimum value. The reported lines come from the connection of all the calculated couple of ratio values.

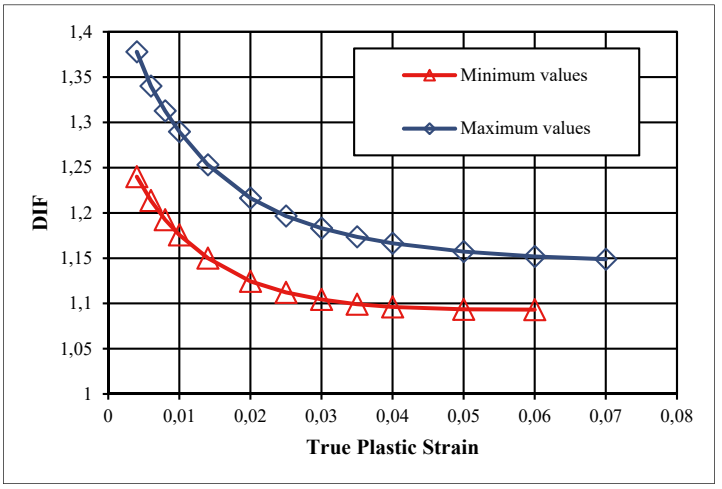

Fig. 4. Dynamic increase factor vs true plastic strain, minimum and maximum values of A component.

Brinell hardness tests HBW 2.5/62.5 were performed on tensile samples. The hardness values are in the range of 48-68 HBW. The relationship between the tensile strength and hardness is shown in Fig. 5; the two properties are proportional as it is reasonable. The lowest hardness values are obtained for samples cut from high wall thickness of

the component C. Analyzing Fig. 5, the obtained experimental data are included between the two dashed lines, evidencing a proportionally bigger percentage change of hardness values in respect than the *TS* values. This fact evidences the usefulness of not destructive hardness test in the evaluation of die cast components mechanical characterization.

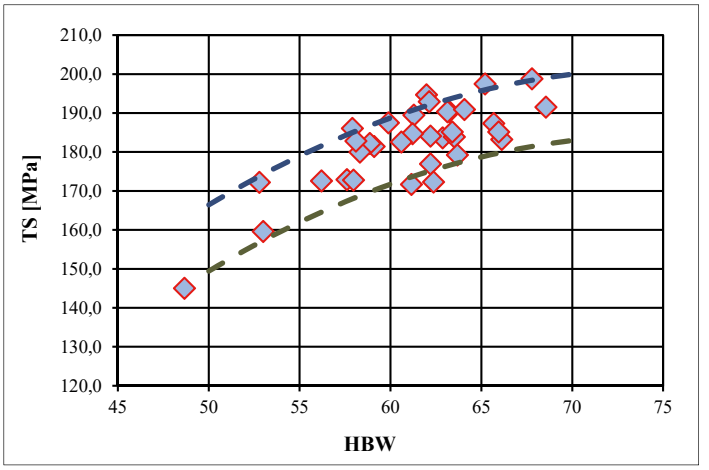

Fig. 5. Tensile strength versus HBW.

The observation at low magnification of fracture surfaces of static and dynamic tensile samples with SEM evidences a rough morphology that suggests that fracture occurred in a brittle manner in the most part of samples. At higher magnification, a general lack of ductile behaviour is also confirmed from the absence of shear lips on the edges of fracture surfaces. Nevertheless, at magnification around 1000X it is possible to see the presence of fine dimples and a high amount of bigger voids, produced by plastic deformation induced around Si particles and brittle (Al- Fe- Mn- Si) phase, on the fracture surface. The coalescence of fine and coarse voids, often passing through the shrinkage porosity that contains dendrite lobes, produces the surface morphology shown in Fig. 6a. This image was taken on a specimen of component C, static tensile tested.

In case of dynamic tests, the fracture morphology at high magnification – Fig. 6b, component A – evidences the presence of coarse pores coalescences that however are not mainly localized on the fracture surface, but seem to have an almost 3-dimensional distribution. Certain amounts of brittle morphology are however detected.

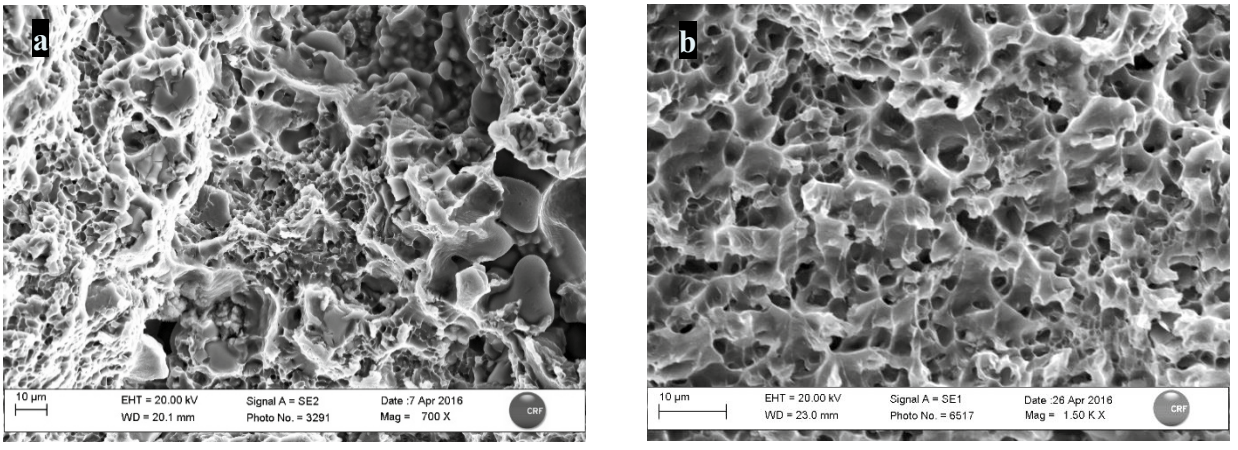

Fig. 6. Fracture morphology of a sample of compound C (a) 2.3 % e_f - static test and of component A (b) 28.4 % e_f - dynamic test.

This latter morphology can justify the higher percentage amount of plastic deformation, above the maximum load, generally detected in samples undergone dynamic tests.

4. Conclusions

The research, carried out on die cast products in AlSi10MnMg, shows a slight increase in mechanical properties of the alloy, at high strain rate in respect to quasi-static tests. This increase is not however constant, but depends on plastic strain amount. Contemporarily, at high strain rate, this alloy evidences a remarkable increase in the total fracture elongation (e_f), mainly connected with higher strain beyond the *TS*, when necking starts.

The fracture analysis evidences a different morphology in the comparison between quasi-static and dynamic tensile specimens.

The metallographic observations show a not homogenous microstructure and porosity distribution that can justify the sometimes wide data scattering of e_f obtained in some components.

Further analyses are scheduled to improve the knowledge of this alloy in case of high strain rate.

References

Schultz, R., 2008. Aluminium Association Auto and Light Truck Group 2009 Update on North American Light Vehicle Aluminium Content Compared to the other Countries and Regions of the World. Phase II, Ducker Worlwide LLC. Troy, MI, USA, 8-19.

Franke, R., Dragulin, D., Zovi, A., Casarotto, F., 2007. Progress in ductile aluminium high pressure die casting. La Metallurgia Italiana, memorie, die casting, 21-27.

Kaufman, J. G., Rooy, E. L., 2004. Aluminum Alloy Castings: Properties, Processes, and Applications. First edition, (Ed). ASM International.

Vicario, I., Crespo, I., Plaza, L. M., Caballero, P., Idoiaga, I. K., 2016. Aluminium Foam and Magnesium Compound Casting Produced by High-Pressure Die Casting. Mdpi journal, metals.

Avalle, M., Belingardi, G., Cavatorta, M. P., Doglione, R., 2002. Casting defects and fatigue strength of a die cast aluminium alloy: a comparison between standard specimens and production components. International Journal of Fatigue 24, 1–9.

Cáceres, C. H., Selling, B. I., 1996. Casting defects and the tensile properties of an A1-Si-Mg alloy. Materials Science and Engineering A220, 109-116.

Niklas, A., Bakedano, A., Orden, S., da Silva, M., Noguésc, E., Fernández-Calvo, A. I., 2015. Effect of microstructure and casting defects on the mechanical properties of secondary AlSi10MnMg(Fe) test parts manufactured by vacuum assisted high pressure die casting technology. Materials Today, proceeding 2, 4931- 4938.

Ubertalli, G., Rosalbino, F., Matteis, P., Scavino, G., Firrao, D., Scandaliato, F., 2015. Caratterizzazione di leghe Zama 2 pressocolate in riferimento a fenomeni connessi con l'invecchiamento. La Metallurgia Italiana, materiali non ferrosi, 33-41.

Mirone, G., 2013. The dynamic effect of necking in Hopkinson bar tension tests. Mechanics of Materials 58, 84-96.

Kolsky, H., 1949. An investigation of the mechanical properties of materials at very high rates of loading. Proceedings of the Physical Society. Section B, 62(11), 676-700.

Albertini, C., Montagnani, M., 1974. Testing techniques based on SHPB. Institute of Physics Conference series No. 21, 22–32.

Vilamosa, V., Clausen, A. H., Børvik, T., Skjervold, S. R., Hopperstad, O. S., 2015. Behaviour of Al-Mg-Si alloys at a wide range of temperatures and strain rates. International Journal of Impact Engineering 86, 223-239.

Ma, H., Huang, L., Tian, Y., Li, J., 2014. Effects of strain rate on dynamic mechanical behavior and microstructure evolution of 5A02-O aluminum alloy. Materials Science & Engineering A 606, 233-239.

Smerd, R., Winkler, S., Salisbury, C., Worswick, M., Lloyd, D., Finn, M., 2005. High strain rate tensile testing of automotive aluminium alloy sheet. International Journal of Impact Engineering 32, 541-560.

Tan, J. Q., Zhan, M., Liu, S., Huang, T., Guo, J., Yang, H., 2015. A modified Johnson–Cook model for tensile flow behaviors of 7050-T7451 aluminum alloy at high strain rates. Materials Science & Engineering A 631, 214-219.

Singh, N. K., Cadoni, E., Singha, M. K., Gupta, N. K., 2013. Dynamic Tensile and Compressive Behaviors of Mild Steel at Wide Range of Strain Rates. Journal of Engineering Mechanics 139, 1197-1206.

Ludwik, P., 1909. Elemente der technologischen Mechanik. Springer Verlag Berlin.

D'Aiuto, F., De Caro, D., Federici, C., Tedesco, M. M., Ziggiotti, A., Cadoni, E., 2015. Application of the dynamic characterization of metals in automotive industry. EPJ Web of Conferences 94, 05002.